ADVANCING EARTH AND SPACE SCIENCE

JGR Oceans

RESEARCH ARTICLE

10.1029/2021JC017264

Key Points:

- Laboratory data are used to assess the validity of wave setup predictions following linear and nonlinear approaches
- In a wave-by-wave analysis wave setup predictions are greatly improved when accounting for short-wave nonlinearity
- Linear wave setup predictions are improved using spectral instead of wave-by-wave approach due to a correct account of the wave energy

Correspondence to:

T. Guérin,
thomas.guerin@bw-cgc.fr

Citation:

Guérin, T., & Ruessink, G. (2021). Can short-wave nonlinearity affect the prediction of wave setup? *Journal of Geophysical Research: Oceans*, *126*, e2021JC017264. https://doi.org/10.1029/2021JC017264

Received 9 FEB 2021
Accepted 4 AUG 2021

Can Short-Wave Nonlinearity Affect the Prediction of Wave Setup?

Thomas Guérin[1] and Gerben Ruessink[2]

[1]BW-CGC (Benoit Waeles - Consultant Génie Côtier), Brest, France, [2]Department of Physical Geography, Faculty of Geosciences, Utrecht University, Utrecht, The Netherlands

Abstract Based on high-resolution laboratory data of instantaneous surface elevation and fluid velocity associated with the propagation of short waves over a gently sloping beach (GLOBEX project), the present work compares two methods for predicting the wave setup. A one-dimensional (cross-shore) model is considered to solve the balance equation that links the pressure gradient induced by the mean surface elevation profile with the wave radiation stress (including wave roller) and bottom stress profiles. When compared to measurements and using a wave-by-wave approach, the mean elevation appears to be significantly better predicted with a nonlinear approach based on stream function theory than with the commonly used linear approach based on Airy wave theory. At the shoreline, the linear method overestimates the wave setup by at least about 50% while this error is globally reduced by a factor 2 to 4 in the nonlinear case. In the framework of this study, the combined contribution of bottom stress and wave roller to the wave setup appears secondary since it accounts for about 10% of the predicted setup at the shoreline. Alternative computational methods are also considered to model the wave setup. In the linear case, using a spectral instead of the wave-by-wave approach greatly improves the wave setup predictions. This improvement is related to the disparity between the representative wave height (and thus the wave energy) obtained from spectral and wave-by-wave analysis when short-wave nonlinearity becomes significant.

Plain Language Summary The breaking of waves near the shore increases the mean sea level to a maximum at the shoreline. This so-called wave setup is of fundamental importance in coastal dynamics, especially regarding flooding issues during storm events. Here, we use laboratory measurements of surface elevation and fluid velocity associated with waves propagating over a uniform beach to test the validity of wave setup predictions following two different approaches. The first one is based on the basic and common framework within which the waves are always represented by sinusoids, while the second one is based on a more elaborate and realistic representation of waves. We show that using the basic approach significantly overestimates the wave setup, while the more elaborate approach leads to more realistic predictions.

1. Introduction

The wave setup, defined here as the maximum increase in mean sea level at the shoreline due to breaking waves, was already observed more than 50 years ago (e.g., Bowen et al., 1968; Savage, 1957; Saville, 1961). Its importance in coastal dynamics has been widely reported, especially regarding extreme water levels during storm events (Guérin et al., 2018; Kennedy et al., 2012; Mastenbroek et al., 1993; Nicolae-Lerma et al., 2017; Wolf, 2009), but also in relation to estuarine and tidal inlet dynamics (Bertin et al., 2009; Fortunato et al., 2017), or to the process of undertow and thus to morphological changes of the beach profile (Dally & Dean, 1984; Dyhr-Nielsen & Sørensen, 1970). Modeling wave setup is commonly performed through the use of spectral wave models in 2DH or 3D configurations (e.g., Wu et al., 2018; Ye et al., 2020), while it can also be done considering a simpler 1D cross-shore configuration where the balance equation between the wave-induced momentum flux and pressure gradient is solved (e.g., Apotsos et al., 2007; Raubenheimer et al., 2001). Yet only little attention has been paid to the fact that, for the most part, modeling wave setup from a phase-averaged approach remains inherently based on the consideration of linear sinusoidal waves (i.e., according to Airy wave theory). This is obviously a crude approximation in the shoaling and breaking zone, which leaves us with the question of whether considering nonlinear waves (rather than linear waves) does impact the prediction of wave setup.

James (1974) pioneered the consequences of considering nonlinear (hyperbolic and Stokes) waves for computing the wave setup. His study, which applies to spilling breakers on gently sloping beaches only, concludes that momentum fluxes at the break point computed from Airy waves and from nonlinear waves are of the same order for a wide range of wave conditions, leading to small differences in terms of wave setup. However, Stive and Wind (1982) found that using elaborate nonlinear methods for computing the wave radiation stress from measurements of surface elevation and velocity field leads to improved predictions of wave setup compared to using the linear wave theory, in their case for periodic and normally incident waves on a gently sloping beach. Svendsen (1984) considered a simpler approximation for the wave shape (which can be referred to as a second-order formulation) and at the same time introduced the effect of the wave roller in the surf zone. His results mostly highlighted the importance of the roller in the radiation stress computation, and thus in the wave setup computation, but did not clearly consider the effect of the wave shape on wave setup. Wang et al. (2008) investigated the latter effect by approximating the wave shape up to the sixth-order while relaxing the small wave amplitude assumption in Svendsen (1984) and also accounting for the roller. They obtained lower values of radiation stress compared to those computed with second-order waves, leading to slightly smaller wave setup predictions (with average differences of maximum setup between simulations and measurements less than 15%), but unfortunately without direct comparisons with predictions based on linear waves. Another approach was proposed by Shabani et al. (2011) based on nonlinear shallow water wave theory, where the main difference with the model of Wang et al. (2008) is the consideration of a variable wave celerity within a wave period instead of a constant one (i.e., taking this celerity to be $\sqrt{g(h+\eta)}$ instead of $\sqrt{gh}$, where g, h and η are the gravitational acceleration, the water depth and the instantaneous surface elevation, respectively). The latter assumption allowed to take into account the inherent mechanism of shape variation as waves propagate onshore, rather than considering a user-defined wave shape parameter as in Svendsen (1984) and Wang et al. (2008). With their nonlinear approach, Shabani et al. (2011) obtained smaller values of wave radiation stress compared to the linear approach, and globally better estimations of the mean elevation cross-shore profile. Because their method uses the measured mean elevation at the shoreline as the starting point for their computations, only the (cross-shore) slope of the predicted mean elevation profiles can be compared (i.e., perfect agreement between measured and predicted setup at the shoreline is automatically obtained following this method). But their work still implies that linear theory should significantly overestimate the wave setup at the shoreline because of a too high cross-shore gradient of mean elevation, while largely overestimating the set-down. When focusing on the prediction of the undertow over a barred beach, Garcez Faria et al. (2000) did succinctly look at the effect of linear or nonlinear waves in setup computations. They also obtained lower radiation stress and therefore less set-down when considering nonlinear waves, but without significant alteration of the mean elevation profile compared to the linear case probably because of the significant contribution from the momentum flux of the mean current (i.e., strong undertow associated with storm events). Numerical simulations of wave setup at a reef-lagoon system were recently shown by Rijnsdorp et al. (2021) using the phase-resolving model SWASH, which intrinsically capture the short-wave nonlinearity. The increase of bottom stress due to the account of nonlinear wave shapes is highlighted in their study. Concurrently, some studies showed that there are cases where the wave setup is acceptably predicted using a phase-averaged approach and following the radiation stress concept based on linear wave theory (e.g., Buckley et al., 2015). The potential impact of short-wave nonlinearity on the prediction of wave setup thus remains unclear.

The main goal of the present study is to examine the role of short-wave nonlinearity on wave setup, using a one-dimensional cross-shore model based on either the linear wave theory or the stream function representation of waves initially introduced by Dean (1965) and eventually improved by Fenton (1999). Section 2 presents the one-dimensional cross-shore equation considered to compute the wave setup, and the linear and nonlinear approaches employed to compute the fluid characteristics (i.e., instantaneous surface elevation, orbital velocity and pressure) required to the radiation stress computation. The model implementation is presented in Section 3. Comparisons between theoretical predictions and measurements from the GLOBEX laboratory experiments (Ruessink et al., 2013) are presented in Section 4, regarding instantaneous surface elevation and horizontal velocity over a wave cycle, and mean elevation profile. The respective contribution of bottom stress and wave roller on the setup is then investigated in Section 5, as well as alternative methods to compute the wave radiation stress. Conclusions are given in Section 6.

2. Theoretical Framework

2.1. General Model

The one-dimensional time-averaged cross-shore balance equation between the depth-averaged wave momentum flux associated with the shore-normal propagation of short waves and the bottom stress, and the pressure gradient associated with the mean surface elevation profile, is (Stive & Wind, 1982):

$$\frac{\partial S_{xx}}{\partial x} + \tau_b = -\rho g h \frac{\partial \overline{\eta}}{\partial x}, \tag{1}$$

where x is the cross-shore coordinate (positive onshore), S_{xx} the wave radiation stress, τ_b the bottom stress, ρ the water density, g the gravitational acceleration, $h = d + \overline{\eta}$ the total water depth with d being the still water depth and $\overline{\eta}$ the mean surface elevation (the overbar denoting the time average over several waves). The advection term due to the mean flow is absent in Equation 1 since the time-averaged mass flux is zero for a closed wave flume with impermeable bottom such as in GLOBEX experiments (Stive & Wind, 1986). The wave radiation stress term includes the wave roller contribution:

$$S_{xx} = S_{xx,w} + S_{xx,r}, \tag{2}$$

where $S_{xx,w}$ is the excess flow of momentum due to the presence of (nonbreaking) waves as defined by Longuet-Higgins and Stewart (1964), and $S_{xx,r}$ denotes the additional flow of momentum related to the wave roller energy, i.e. associated with the volume of water carried shorewards with the breaker as defined by Svendsen (1984). According to its primary integral definition (Equation 7 of Longuet-Higgins & Stewart, 1964), the computation of $S_{xx,w}$ reads:

$$S_{xx,w} = \overline{\int_{-d}^{\eta} (p + \rho u^2)\, dz} - \int_{-d}^{\overline{\eta}} p_0\, dz, \tag{3}$$

where z is the vertical coordinate (positive upward from the still water level), p the instantaneous pressure at any point within the fluid, $p_0 = -\rho g(z - \overline{\eta})$ the hydrostatic pressure (neglecting atmospheric pressure), and u the horizontal component of the instantaneous orbital velocity in the cross-shore direction. However, the following expression is employed in the present work to correctly account for the dynamic pressure contribution when the pressure is obtained from linear theory (Equation 19 of Stive & Wind, 1982):

$$S_{xx,w} = \int_{-d}^{\eta_c} (\rho \overline{u^2} - \rho \overline{w^2})\, dz + \frac{1}{2} \rho g \overline{\left(\eta - \overline{\eta}\right)^2}, \tag{4}$$

where η_c is the level of the wave crest, and w is the vertical component of the instantaneous orbital velocity.

According to Svendsen (1984), the additional source of radiation stress due to the wave roller for shore-normal waves is:

$$S_{xx,r} = 2E_r, \tag{5}$$

where E_r is the roller energy. As shown by Martins et al. (2018), the related energy dissipation can be significantly overestimated when directly computing E_r through an empirical parametrization of the roller area and density (e.g., using Equations 11 and 12 of Lippmann et al., 1996). In this study the roller energy is computed following the energy balance equation (Buckley et al., 2015):

$$\frac{\partial}{\partial x}\left(2E_r c\right) = D_{br} - \frac{2gE_r}{c} \beta_D, \tag{6}$$

where c is the phase velocity, $\beta_D = \sin(\theta_r)$ with θ_r the angle of the wave/roller stress vector (i.e., the wave front slope angle) as in Apotsos et al. (2007), and the wave-breaking dissipation D_{br} is defined as:

$$D_{br} = -\frac{\partial \overline{F_w}}{\partial x}, \tag{7}$$

where $\overline{F_w}$ is the wave energy flux. The latter can be estimated according to Equation 5.5.10 of Holthuijsen (2010):

$$\overline{F_w} = \overline{\int_{-d}^{\eta} \mu \left(p + \frac{1}{2} \rho g \left(u^2 + w^2\right) + \rho g z \right) dz}. \tag{8}$$

The method of Malarkey and Davies (2012), based on Soulsby and Clarke (2005), is used to compute the bottom stress. It allows for the possibility of computing τ_b based on a current measurement at a particular height above the bed, as it is the case for the GLOBEX measurements considered in the present study. More precisely, τ_b is defined as the (wave cycle) mean bottom stress under combined waves and current:

$$\tau_b = \rho u_{*m}^2, \tag{9}$$

where the mean shear velocity u_{*m} is computed as:

$$u_{*m} = \sqrt{\left(\frac{u_{*e}\log(h/e\delta)}{2\log(\delta/z_0)}\right)^2 + \frac{u_{da}u_{*e}\kappa}{\log(\delta/z_0)}} - \frac{u_{*e}\log(h/e\delta)}{2\log(\delta/z_0)}, \tag{10}$$

where $\kappa = 0.4$ is the von Kármán constant, u_{*e} is the effective friction velocity, δ is the wave boundary layer thickness, z_0 is the bed roughness length, u_{da} is the depth-averaged current estimated from the current measurement available at a particular height above the bed and assuming a two-stage logarithmic profile, and $e = \exp(1)$. For more details, the reader is referred to Malarkey and Davies (2012).

2.2. Linear Approach

The linear approach considered in the present study is based on the Airy solution for small-amplitude waves over a flat bottom, which leads to the following expressions for the instantaneous surface elevation (η_l), horizontal and vertical orbital velocity components (u_l and w_l), and pressure (p_l):

$$\eta_l(x,t) = a\cos(k_l x - \omega t), \tag{11}$$

$$u_l(x,z,t) = a\omega\frac{\cosh(k_l(z+h))}{\sinh(k_l h)}\cos(k_l x - \omega t), \tag{12}$$

$$w_l(x,z,t) = a\omega\frac{\sinh(k_l(z+h))}{\sinh(k_l h)}\sin(k_l x - \omega t), \tag{13}$$

$$p_l(x,z,t) = p_0(z) + \rho g a\frac{\cosh(k_l(z+h))}{\cosh(k_l h)}\cos(k_l x - \omega t), \tag{14}$$

where $a = H/2$ is the wave amplitude, $\omega = 2\pi f = 2\pi/T$ is the wave angular frequency (f and T being the wave frequency and period, respectively), and k_l is the wavenumber according to the linear dispersion relation. The associated phase velocity is

$$c_l(x) = \omega/k_l(x). \tag{15}$$

Equations 11–13 are used to compute $S_{xx,w}$ through Equation 4, while Equations 11–15 are used to compute $S_{xx,r}$ through Equations 5–8.

2.3. Nonlinear Approach

In the present work, the method of Fenton (1999) is used to obtain the fluid characteristics (i.e., pressure, orbital velocities, wave speed) needed to compute the radiation stress term in the nonlinear case. This method is based on the stream function representation of waves introduced by Dean (1965) to obtain the numerical solution of steadily progressing waves on irrotational flow and over a horizontal bed. Similarly to the method of Chappelear (1961), the main feature of this approach is to assume a (truncated) Fourier expansion for the field variable (i.e., the stream function in the present case) so as to satisfy both the field equation throughout the fluid and the bottom boundary condition identically. The problem then reduces to solving a set of nonlinear equations for each Fourier coefficient, for time signal of the surface elevation with values at equi-spaced intervals, as well as for other wave characteristics such as the wave speed. The solution to these equations is finally obtained through successive corrections to an initial estimate, so as to minimize

the errors (in a least-square sense) in the surface boundary conditions. After noticing some unsatisfactory aspects of the initial stream function method (e.g., related to its problematic applicability in deep water, or the impossibility of specifying the mass flux as determining the wave speed), Rienecker and Fenton (1981) developed a numerical method also based on Fourier approximation techniques, but having as its only approximation the truncation of the Fourier series while being valid and applicable from deep to shallow water. An improved version of this method was then given by Fenton (1988) and eventually simplified by Fenton (1999).

Considering the existence, in a 2DV frame, of a stream function $\psi(x,z)$ from which the horizontal and vertical fluid velocity components are derived ($u = \partial\psi/\partial z$, $w = -\partial\psi/\partial x$), the present method is based on the use of a Fourier series when writing the analytical solution for ψ in regard to the Laplace's equation, the bottom and free surface kinematic boundary conditions, and the Bernoulli's equation on the surface:

$$\psi = -\bar{U}(z+h) + \sqrt{\frac{g}{k^3}}\sum_{j=1}^{N}\mathcal{B}_j\frac{\sinh\left(jk(z+h)\right)}{\cosh(jkh)}\cos(jkx), \tag{16}$$

where $\bar{U}$ is the mean (horizontal) flow velocity, $\mathcal{B}_j$ are dimensionless constants, and N is a finite integer that defines the truncation of the Fourier series. This expression for ψ is then used to satisfy the two surface boundary conditions, as well as three other conditions regarding the mean depth, the wave height, and either the wavelength or the wave period and mean current (see Fenton, 1999 for the detailed conditions). A system of $2N+5$ nonlinear equations with $2N+5$ variables is thus obtained and iteratively solved using Newton's method. Basically, it can be written:

$$F_I(\mathbf{y}) = 0 \quad \text{for } I = 1,\ldots,2N+5, \tag{17}$$

where F_I refers to equation I, and $\mathbf{y} = \left\{y_j,\, j = 1,\ldots,2N+5\right\}$ is the vector of all variables. More precisely:

$$\mathbf{y} = \left\{k\eta_1,\ldots,k\eta_{N+1},\mathcal{B}_1,\ldots,\mathcal{B}_{N+1},\bar{U}\sqrt{k/g},kh,Q\sqrt{k^3/g},\mathcal{R}k/g\right\}, \tag{18}$$

where $\eta_1,\ldots,\eta_{N+1}$ is a discretization of the nonlinear instantaneous surface elevation $\eta_{nl}(x,t)$ from wave crest to trough, Q denotes the total volume rate of flow underneath the steady wave per unit length in the direction normal to the (x,z) plane, and $\mathcal{R}$ is a constant relative to the dynamic boundary condition (see Equation 3.4 of Fenton, 1999).

If $\mathbf{y}^{(n)}$ is the approximate solution of (17) after n iterations, $F_I\left(\mathbf{y}^{(n+1)}\right)$ can be written using a Taylor expansion:

$$F_I\left(\mathbf{y}^{(n+1)}\right) \approx F_I\left(\mathbf{y}^{(n)}\right) + \sum_{j=2}^{2N+5}\left(\frac{\partial F_I}{\partial y_j}\right)^{(n)}\delta y_j^{(n)}. \tag{19}$$

Consistent with (17) we want $F_I\left(\mathbf{y}^{(n+1)}\right) = 0$, which gives the following set of linear equations for the unknowns $\delta y_j^{(n)}$:

$$\sum_{j=2}^{2N+5}\left(\frac{\partial F_I}{\partial y_j}\right)^{(n)}\delta y_j^{(n)} = -F_I\left(\mathbf{y}^{(n)}\right) \quad \text{for } I = 1,\ldots,2N+5, \tag{20}$$

which can be solved by standard methods for systems of linear equations, thus obtaining the better approximation $y_j^{(n+1)} = y_j^{(n)} + \delta y_j^{(n)}$ with respect to the previous one $y_j^{(n)}$.

Denoting by k_{nl} the wavenumber obtained with the present nonlinear method, the associated phase velocity is

$$c_{nl}(x) = \omega/k_{nl}(x). \tag{21}$$

The horizontal and vertical velocity components are given by:

$$u_{nl}(x,z,t) = c_{nl} - \bar{U} + \sqrt{\frac{g}{k_{nl}}}\sum_{j=1}^{N}j\mathcal{B}_j\frac{\cosh\left(jk_{nl}(z+h)\right)}{\cosh\left(jk_{nl}h\right)}\cos\left(j(k_{nl}x-\omega t)\right), \tag{22}$$

Table 1
Characteristics of GLOBEX Test Series B (Bichromatic Waves) and R (Random Waves)

Series	a_1 (m)	a_2 (m)	f_1 (Hz)	f_2 (Hz)	T_p (s)	T_g (s)	Remark
B1	0.09	0.01	0.40	0.467	2.308	15	–
B2	0.09	0.01	0.42	0.462	2.268	23.81	–
B3	0.07	0.03	0.42	0.462	2.268	23.81	–
R1	0.05	–	–	–	1.60	–	$\gamma_j = 3.3$
R2	0.10	–	–	–	2.25	–	$\gamma_j = 3.3$
R3	0.05	–	–	–	2.25	–	$\gamma_j = 20$

Note. Offshore amplitudes and frequencies of the two short-wave trains for series B are, respectively, a_1 and a_2, and f_1 and f_2, while T_p is the short-wave peak period and T_g is the group period. For series R, the offshore wave amplitude a_1 corresponds to $H_s/2$, while γ_j denotes the JONSWAP peak enhancement factor.
GLOBEX, Gently sLOping Beach EXperiments.

$$w_{nl}(x,z,t) = \sqrt{\frac{g}{k_{nl}}}\sum_{j=1}^{N} j\mathcal{B}_j \frac{\sinh\left(jk_{nl}(z+h)\right)}{\cosh\left(jk_{nl}h\right)}\sin\left(j(k_{nl}x-\omega t)\right), \tag{23}$$

while the pressure at any point within the fluid is:

$$p_{nl}(x,z,t) = \rho\left(\mathcal{R} - gz - \frac{1}{2}\left((u_{nl}-c_{nl})^2 + w_{nl}^2\right)\right). \tag{24}$$

Consistent with the linear approach, Equations 22 and 23 (together with η_{nl}) are used to compute $S_{xx,w}$ through Equation 4, while Equations 21–24 (together with η_{nl}) are used to compute $S_{xx,r}$ through Equations 5–8.

Note that this nonlinear approach solves for wave skewness but does not account for wave asymmetry (i.e., the forward leaning of the wave shape).

3. Observations and Model Implementation

3.1. The GLOBEX Data Set

The Gently sLOping Beach EXperiments (GLOBEX) were performed in the Scheldt flume of Deltares (Delft, the Netherlands) in 2012, and are extensively described in Ruessink et al. (2013). The flume was 100 m long, with as experimental setup a horizontal part with 85 cm water depth at the wave maker, followed by a fixed beach slope of 1:80 over the other 85% of the flume. The wave maker position corresponds to $x = 0$, and the position of the still water shoreline, hereafter simply referred as the shoreline, is $x = 84.6$ m (de Bakker et al., 2015). The median grain size d_{50} of the employed material used to cover the concrete bed was 0.75 mm. To avoid re-reflection of waves at the wave maker, an active reflection compensation was used. Sea-surface elevation measurements were taken at 190 locations (obtained by relocating most of the 21 wave gauges before repeating an experiment, 10 times), together with velocity measurements at 43 locations. The height of the current meters above the bed varied between 0.01 and 0.3 m, depending on location within the flume. The sampling frequency of the instruments was 128 Hz. The GLOBEX experiments comprised three bichromatic and three random wave conditions, called here test series B and R, respectively. Their characteristics are summarized in Table 1.

3.2. Model Implementation

The one-dimensional cross-shore grid considered in our model is composed by the locations where measurements of both the surface elevation and the fluid velocity are available, since these two parameters are used as inputs at some point in the model. A wave-by-wave approach is then considered to compute S_{xx} and τ_b relative to each individual wave and at each grid point, by performing a zero-crossing analysis (see Section 3.3 for more details). The fluid characteristics η, u, w, and p over each wave cycle are modeled following the linear and nonlinear methods presented in Section 2, using the measured water depth and individual wave height and period as input parameters. Each wave cycle is represented by $2N$ bins, where $N = 30$ is the number of Fourier coefficients selected in our case for the nonlinear approach.

As previously mentioned, computation of $S_{xx,w}$ in the linear and nonlinear cases is done according to Equation 4 (since using Equation 3 would not account for the dynamic pressure contribution in the linear case), for each individual wave. Note that a sensitivity analysis led us to use a vertical discretization of $dz = 0.01$ m for performing numerical integration in Equation 4 (as well as in Equation 8 for the roller). Once $S_{xx,w}$ is estimated for each wave, its mean value (i.e., over the total number of waves) is computed for both approaches at each grid point.

To obtain the additional radiation stress due to wave roller ($S_{xx,r}$), the related energy balance equation is solved explicitly based on the method of Dally and Brown (1995) (see their Equation 14), which leads to:

$$E_{r,i+1} = \left[\overline{F_{w,i}} - \overline{F_{w,i+1}} + E_{r,i}\left(2c_i - \frac{g\beta_{D,i}\Delta x_{i+1}}{c_i}\right)\right]\left(2c_{i+1} + \frac{g\beta_{D,i+1}\Delta x_{i+1}}{c_{i+1}}\right)^{-1}, \tag{25}$$

where i denotes the grid point, $\Delta x_{i+1} = x_{i+1} - x_i$, and taking $E_{r,i} = 0$ for $x_i \leq x_{b,off}$ as boundary condition, with $x_{b,off}$ being the offshore limit of the breaking zone. Note that, contrary to $S_{xx,w}$, E_r is not obtained for each individual wave since it would require to track each wave along the cross-shore direction because of using an energy balance equation. Consequently, mean values of $\overline{F_w}$, c and β_D are considered in Equation 25, so that E_r (and thus $S_{xx,r}$) already corresponds to the mean value over the total number of waves at each grid point. Specifically, c_l together with $\overline{F_w}$ based on Equations 11–14 are used in the linear case, while c_{nl} together with $\overline{F_w}$ based on Equations 22–24 are used in the nonlinear case. As for β_D, the value obtained from the nonlinear method is used in both cases since considering the value corresponding to sinusoidal waves in the linear case leads to unrealistically high values of E_r (not shown).

The bottom stress relative to each wave is computed according to Equations 9 and 10 with the measured wave period and the wave-averaged measured current at a particular height as input parameters. The bed roughness is defined by the grain roughness following the relation $z_0 = d_{50}/12$. The modeled orbital velocity amplitude obtained from the linear and nonlinear methods are considered separately to compute τ_b in both cases. Similar to $S_{xx,w}$, once τ_b is estimated for each wave its mean value is computed for both approaches at each grid point.

The mean profiles of S_{xx} and τ_b are eventually used to compute the mean elevation profile, which is done by solving Equation 1 following a finite difference scheme centered in space:

$$\overline{\eta}_{i+1} = -\frac{(S_{xx,i+1} - S_{xx,i-1}) + \tau_{b,i}(x_{i+1} - x_{i-1})}{\rho g h_i} + \overline{\eta}_{i-1}. \tag{26}$$

The seaward boundary condition imposes the modeled mean surface elevation to be equal to the measured one at the two most offshore grid points. A computational loop is also performed to ensure the convergence of the solution (typically reached for less than five iterations), since $\overline{\eta}$ comes up explicitly in the right-hand side of Equation 26 through both $\overline{\eta}_{i-1}$ and the total water depth $h_i = d + \overline{\eta}_i$.

Note that the measured individual wave heights and periods are directly used for the computation of instantaneous surface elevation, orbital velocity and pressure, which removes the potential source of error due, for instance, to using modeled wave heights and periods. Also, the present wave-by-wave approach was chosen in order to make the most use of the available experimental data. Alternative approaches are considered and discussed in Section 5.

3.3. Data Processing

The first five minutes of each GLOBEX experiment are considered for the computations. This time scale is typically an order of magnitude larger than the infragravity (IG) time scale since the (peak) group period is less than 30 s for all experiments (see Table 1 for group periods associated with the bichromatic wave conditions and see Guérin et al. (2019) for peak group periods associated with the random wave conditions). Because the two theoretical methods employed in this work to model the instantaneous surface elevation and fluid velocity apply to short waves, only the short-wave frequency band of the measurements is used in the wave-by-wave approach when it comes to wave height and period, which are defined by zero-upcrossing the high-frequency part of the elevation time series. The cutoff between gravity and IG frequencies corresponds to $f_1/2$ for the bichromatic conditions, and follows de Bakker et al. (2015) for the random conditions (i.e., cutoff frequencies of 0.37, 0.26, and 0.26 Hz for series R1, R2, and R3, respectively). At the same time, the total water depth, i.e. including the IG component, is considered in our approach so that, at a given location, each individual wave is experiencing a slightly different water depth (as in reality).

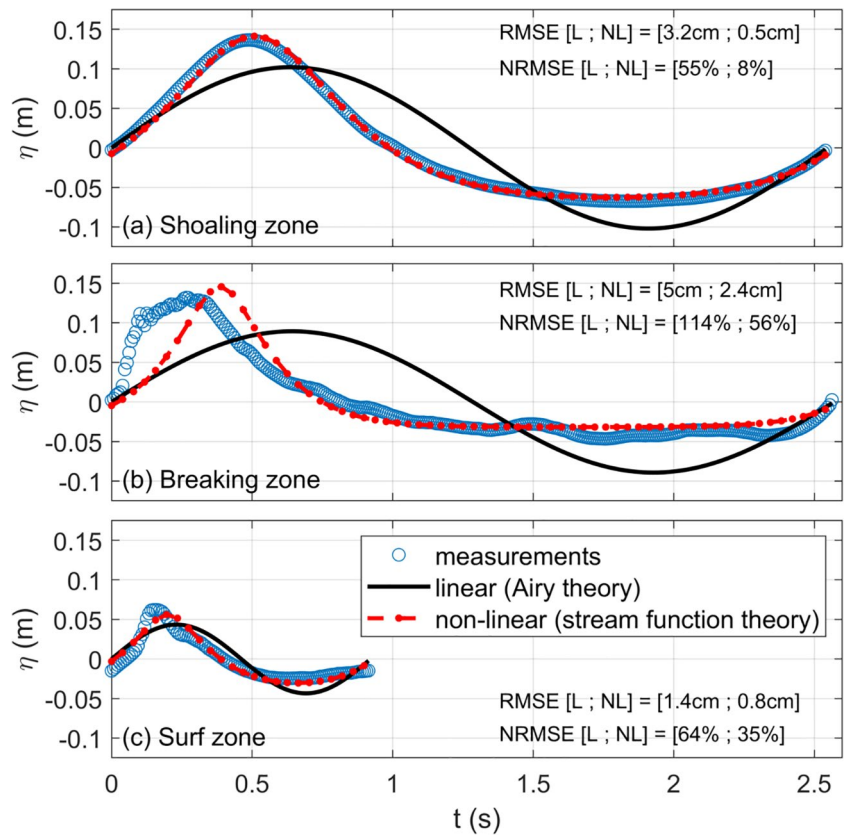

Figure 1. Example of comparison between measured and predicted instantaneous surface elevation during a wave cycle for GLOBEX series B1. The three presented individual waves are extracted during the first 15 s of the experiment, while the associated cross-shore positions correspond approximately to the center of the three zones (see Figure 2 for the visualization of their delimitations).

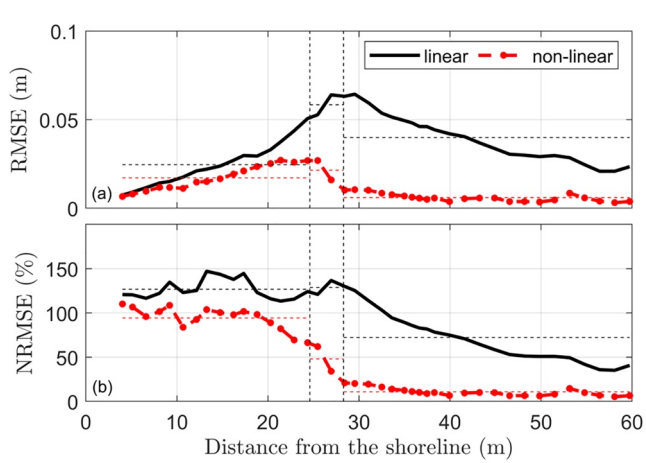

Figure 2. Cross-shore profiles of root-mean-square errors (a) and normalized root-mean-square errors (b) computed for the instantaneous surface elevation over the first 5 min of GLOBEX series B1 (which gives about 120–300 individual waves when going from the shoaling to the surf zone). Vertical dashed lines delimit the three zones, while horizontal dashed lines correspond to the mean error value for each zone and both methods.

Going from individual waves to overall error statistics is done by computing the predictive skills of the linear and nonlinear methods in terms of root-mean-square errors (RMSE) and normalized root-mean-square errors (NRMSE) following, for η:

$$RMSE\ (x_i) = \frac{1}{M_i}\sum_{m=1}^{M_i}\sqrt{\frac{1}{2N}\sum_{j=1}^{2N}\left(\eta_{pred,i,m}(j) - \eta'_{meas,i,m}(j)\right)^2}, \tag{27}$$

$$NRMSE\ (x_i) = \frac{1}{M_i}\sum_{m=1}^{M_i}\left(\frac{\sqrt{\frac{1}{2N}\sum_{j=1}^{2N}\left(\eta_{pred,i,m}(j) - \eta'_{meas,i,m}(j)\right)^2}}{\frac{1}{2N}\sum_{j=1}^{2N}\mid \eta'_{meas,i,m}(j)\mid}\right), \tag{28}$$

where M_i is the number of waves detected by the zero-upcrossing function at grid point i in the 5-minute time series, while $\eta_{pred,i,m}(j)$ and $\eta'_{meas,i,m}(j)$ are the predicted and measured instantaneous surface elevation corresponding to the short-wave frequency band at grid point i and associated with wave m and bin j of the wave cycle, respectively. The error statistics related to the instantaneous horizontal velocity are computed in a similar manner. The smaller the NRMSE, the closer the agreement between predictions and measurements.

Table 2
NRMSE Associated to the Instantaneous Surface Elevation Predicted With the Linear (L) and Nonlinear (NL) Methods, and Averaged by Zones

	Shoaling zone		Breaking zone		Surf zone	
Series	L	NL	L	NL	L	NL
B1	72%	11%	129%	48%	127%	94%
B2	62%	9%	121%	42%	117%	93%
B3	54%	11%	114%	50%	118%	93%
R1	52%	47%	100%	57%	123%	88%
R2	58%	50%	84%	54%	119%	90%
R3	47%	37%	–	–	112%	69%

Note. NRMSE, normalized root-mean-square errors.

4. Results

Comparisons between measured and predicted instantaneous surface elevation and horizontal velocity over a wave cycle are shown in the following, together with comparisons of measured and predicted mean elevation profile. The shoaling zone (i.e., with only unbroken waves), the surf zone (i.e., where all wave are broken), and the intermediate "breaking zone", which are considered hereafter, are defined based on visual observations as in de Bakker et al. (2015).

4.1. Instantaneous Surface Elevation

Examples of measured and predicted instantaneous surface elevation over a wave cycle are shown on Figure 1 for the three previously defined zones (shoaling, breaking, and surf zone). A significant improvement in representing the evolution of η during an orbital cycle is obtained when using the nonlinear rather than the linear approach. For the three waves shown in Figure 1, the NRMSE decreases from 55% (linear method) to 8% (nonlinear method) in the shoaling zone, from 114% to 56% in the breaking zone, and from 64% to 35% in the surf zone. Note that in the surf zone, the nonlinear method still

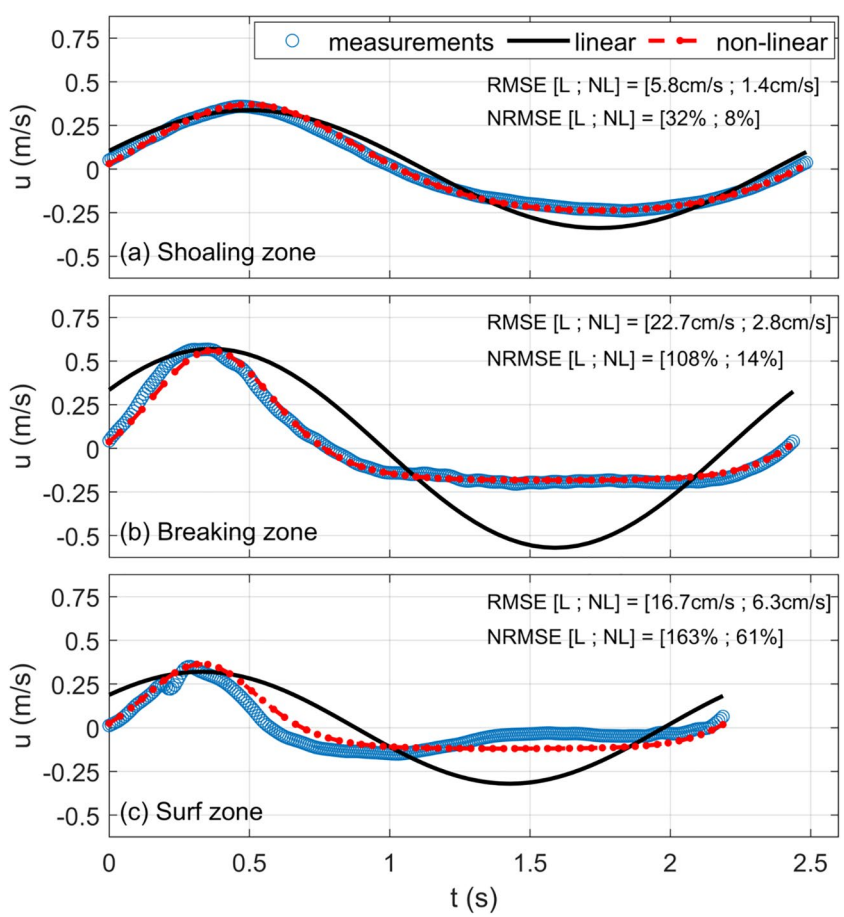

Figure 3. Example of comparison between measured and predicted instantaneous horizontal fluid velocity during a wave cycle for GLOBEX series B1. The three presented individual waves are extracted during the first 15 s of the experiment, while the associated cross-shore positions correspond approximately to the center of the three zones and the associated vertical position of current measurements are 0.05 m, 0.11 m, and 0.01 m above the bed, respectively.

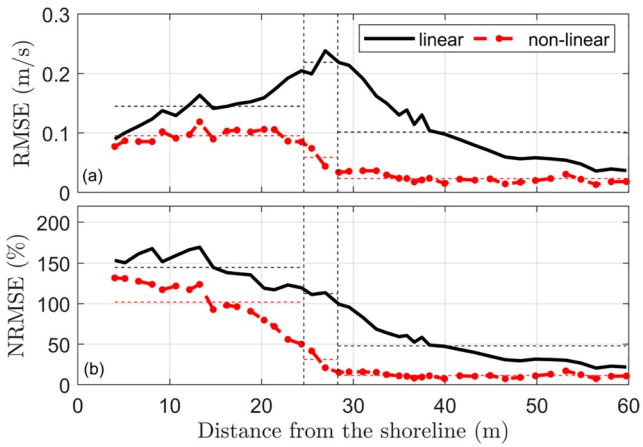

Figure 4. Cross-shore profiles of root-mean-square errors (a) and normalized root-mean-square errors (b) computed for the instantaneous horizontal velocity over the first five minutes of GLOBEX series B1 (which gives about 120–300 individual waves when going from the offshore to the onshore limit). Vertical dashed lines delimit the three zones, while horizontal dashed lines correspond to the mean value for each zone and both methods.

performs better than the linear method despite the fact that wave asymmetry is not represented in the stream function theory.

The overall error statistics (i.e., associated with the 5-min time series) are plotted along the cross-shore axis for GLOBEX series B1 (Figure 2), while Table 2 summarizes these statistics by zone and for all test series. Overall, a systematic improvement in prediction of η is obtained when switching from the linear to the nonlinear method. The associated NRMSE appears significantly reduced especially in the breaking zone for series B and R and in the shoaling zone for series B. The large values of NRMSE obtained with the nonlinear method in the surf zone (69% to 94%) are mainly due to not accounting for wave asymmetry. Note that no error statistic is given in series R3 for the breaking zone, since the latter actually consists in one location because of the narrow-banded spectral shape of the associated wave conditions (de Bakker et al., 2015).

4.2. Instantaneous Horizontal Velocity

Similarly to the orbital surface displacement, the predicted horizontal velocity (u) during an orbital cycle is compared with GLOBEX measurements at every x -location and for each individual wave during the first five minutes of the test series. An example of such comparisons is presented in Figure 3, while the predictive skills of both methods are plotted along the cross-shore axis for GLOBEX series B1 only (Figure 4) and summarized in Table 3 for all test series. As for the surface elevation, the representation of u during an orbital cycle is systematically improved when the nonlinear method is used rather than the linear one.

4.3. Mean Surface Elevation

Example cross-shore profiles of measured and predicted mean surface elevation, together with the associated measured wave height and predicted radiation stress profiles, are shown in Figure 5 for bichromatic conditions (series B1) and in Figure 6 for the most energetic random conditions (series R2). The main observation is the difference of predicted radiation stress between the two approaches, especially when waves reach the breaking zone where S_{xx} appears significantly higher in the linear case. This substantial difference explains the observed overestimation of the wave setup (and set-down for conditions B1) when predicted with the linear approach. The measured and predicted $\overline{\eta}$ at the shoreline, with associated NRMSE at the shoreline and in the surf zone, are summarized in Table 4 for all test series. While the linear approach overestimates $\overline{\eta}$ at the shoreline globally by 50% to 70%, an unequivocal improvement is obtained for all test series when using the nonlinear approach, with a decrease in the related NRMSE globally by a factor 2 to 4. While the decrease in wave radiation stress from linear to nonlinear cases has already been highlighted in previous studies (e.g., Garcez Faria et al., 2000; Shabani et al., 2011; Wang et al., 2008), the improvement we obtain with the nonlinear approach in terms of predicted wave setup especially agrees with the findings of Stive and Wind (1982).

Table 3
NRMSE for the Instantaneous Horizontal Velocity Predicted With the Linear (L) and Nonlinear (NL) Methods, and Averaged by Zones

	Shoaling zone		Breaking zone		Surf zone	
Series	L	NL	L	NL	L	NL
B1	48%	12%	112%	31%	145%	102%
B2	40%	11%	104%	31%	145%	110%
B3	37%	14%	101%	43%	153%	119%
R1	54%	51%	90%	54%	122%	89%
R2	57%	52%	78%	54%	129%	97%
R3	46%	41%	–	–	108%	69%

Note. NRMSE, normalized root-mean-square errors.

5. Discussion

5.1. Contributions of Bottom Stress, Wave Roller and Main Radiation Stress Term to Wave Setup

Apart from the main forcing component associated with the excess flow of momentum due to the presence of waves ($S_{xx,w}$), the two other components influencing the mean elevation profile according to Equation 1 are the bottom stress and the wave roller. As an example, cross-shore profiles of the terms associated to these three forcing components are shown in

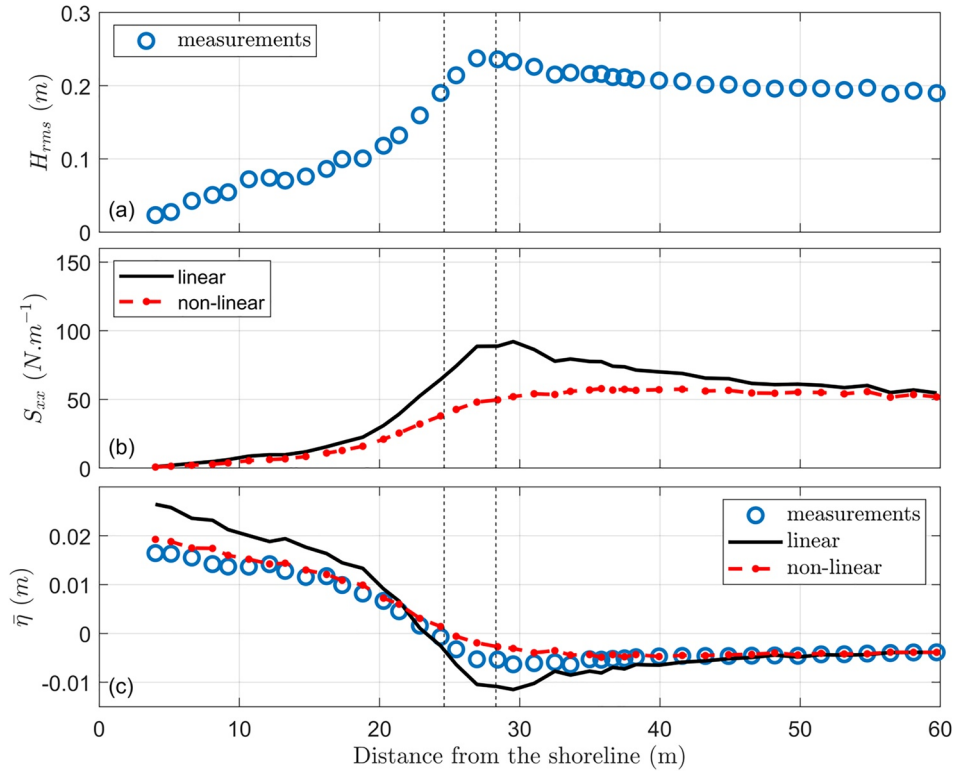

Figure 5. Results for GLOBEX series B1 considering wave-by-wave approach: (a) root-mean-square wave height (measured), (b) wave radiation stress (modeled), and (c) mean surface elevation (measured and modeled).

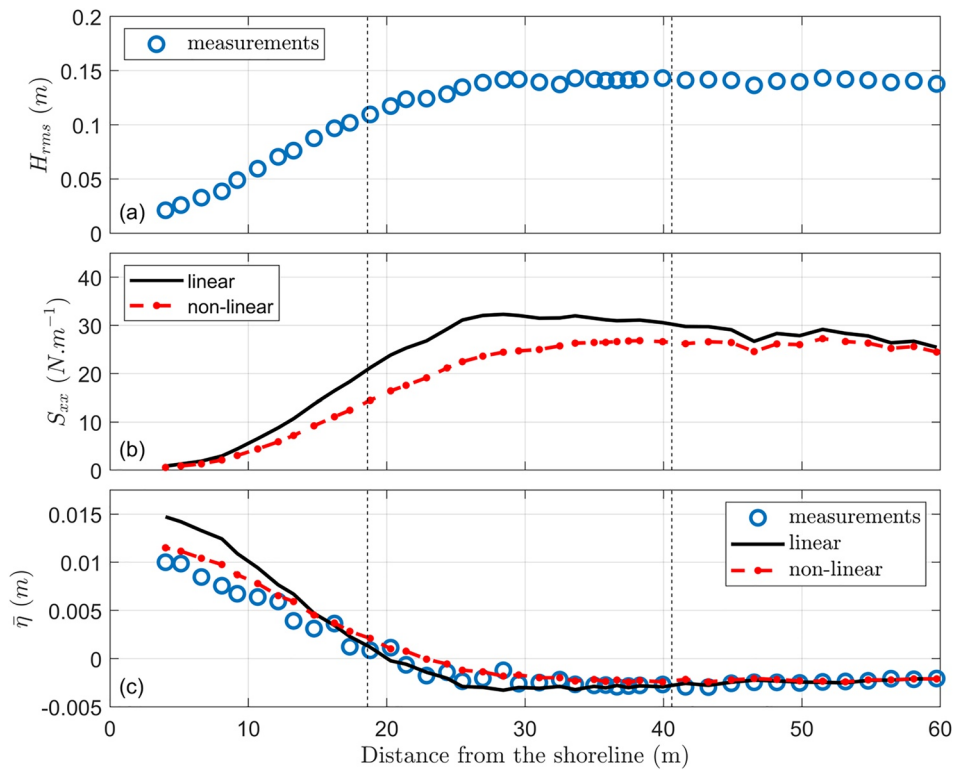

Figure 6. Results for GLOBEX series R2 considering wave-by-wave approach: (a) root-mean-square wave height (measured), (b) wave radiation stress (modeled), and (c) mean surface elevation (measured and modeled).

Figure 7 for GLOBEX series B1, while Figure 8 shows the associated mean elevation profile when modeled with or without the wave roller (upper panel) and with or without the bottom stress (bottom panel), for the two approaches. In absolute value, the bottom stress appears negligible compared to the wave roller term (i.e., $\partial S_{xx,r}/\partial x$) in Figure 7b, but it is seen in Figure 8 that cross-shore integration of both terms leads to a similar decrease in wave setup at the shoreline. This is due to $\partial S_{xx,r}/\partial x$ being negative in the breaking zone but (mainly) positive in the surf zone. As a result, the wave roller contributes to decreasing the mean elevation in the former zone while eventually increasing it in the latter. The detailed results in terms of relative contributions of bottom stress, wave roller and main radiation stress term to the wave setup modeled at the shoreline are summarized in Table 5 for all GLOBEX test series. Overall, the contributions of bottom stress and wave roller appear secondary compared to the contribution of $S_{xx,w}$, since their combined contribution accounts for about 10% of the modeled wave setup at the shoreline, for the two approaches.

5.2. Alternative Computational Methods

Consistent with the enhanced representation of instantaneous surface elevation and fluid velocity over a wave cycle when using stream function rather than linear theory, the prediction of wave setup through a wave-by-wave approach is clearly improved when based on the nonlinear approach (see Figures 5 and 6 and Table 4). Two alternative computational methods are now considered in the present section to compare with the wave-by-wave approach. The first alternative method is to solve Equation 1 based on the bulk wave parameters H_{rms} and T_p. For both the linear and nonlinear cases, a single computation of $S_{xx,w}$ is thus performed at each grid point x_i through Equation 4. The single orbital cycle of η, u, w and p required at each grid point is, for both linear and nonlinear cases, associated with the representative wave defined by the offshore peak period T_p (see Table 1) and the root-mean-square wave height obtained from wave-by-wave analysis as:

$$H_{rms}(x_i) = \sqrt{\frac{1}{M_i}\sum_{m=1}^{M_i} H_{i,m}^2}\,, \tag{29}$$

where M_i denotes the number of individual waves detected at grid point x_i during the time series (see Section 3.3). This hereafter called bulk approach (or bulk computation) differs from the wave-by-wave approach where the mean wave radiation stress at each grid point was obtained by averaging $S_{xx,w}$ computed for each individual wave. Here, consistent with $S_{xx,w}$, a single computation is also performed at each grid point x_i for the roller energy and the bottom stress considering the same representative wave defined by $H_{rms}(x_i)$ and T_p. In the linear case, this bulk computation of $S_{xx,w}$ is equivalent to using Equation 23 of Longuet-Higgins and Stewart (1964):

$$S_{xx,w} = \frac{1}{8}\rho g\, H_{rms}^2\left(\frac{1}{2} + \frac{2kh}{\sinh(2kh)}\right). \tag{30}$$

Table 4
Measured and Predicted Mean Surface Elevation at the Shoreline, With Associated NRMSE

		$\bar{\eta}_{pred}$ and NRMSE (shoreline)		NRMSE (surf zone)	
Series	$\bar{\eta}_{meas}$ (shoreline)	L	NL	L	NL
B1	1.65 cm	2.64 cm; +60%	1.93 cm; +17%	+58%	+17%
B2	1.67 cm	2.58 cm; +54%	1.92 cm; +15%	+57%	+20%
B3	1.28 cm	2.13 cm; +66%	1.59 cm; +24%	+64%	+25%
R1	0.38 cm	0.59 cm; +55%	0.48 cm; +26%	+49%	+25%
R2	1.00 cm	1.47 cm; +47%	1.15 cm; +15%	+56%	+26%
R3	0.47 cm	0.77 cm; +64%	0.55 cm; +17%	+102%	+45%

Note. Linear and nonlinear methods are denoted by L and NL, respectively. NRMSE for the surf zone is also mentioned. NRMSE, normalized root-mean-square errors.

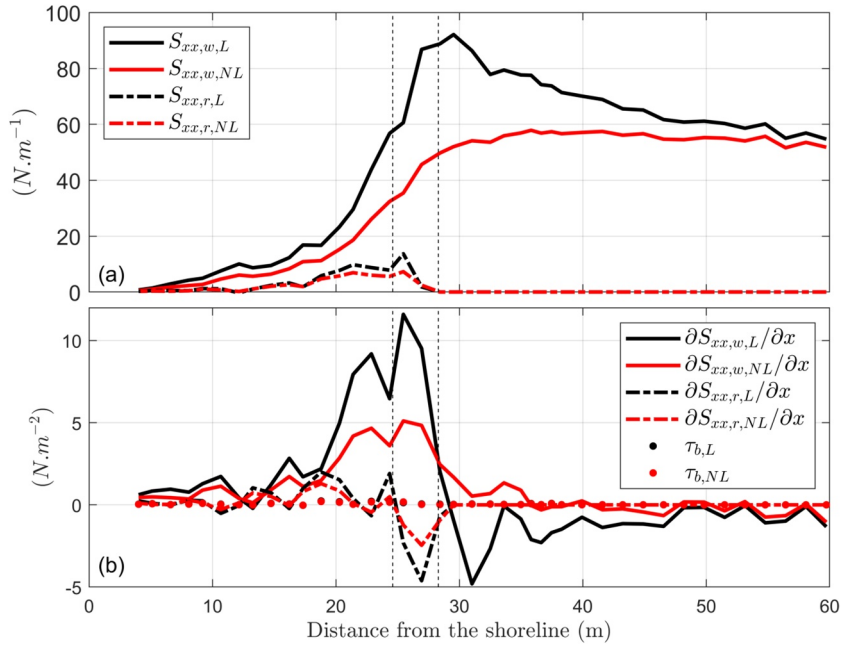

Figure 7. Cross-shore profiles of (a) $S_{xx,w}$ and $S_{xx,r}$, and (b) τ_b and gradient of $S_{xx,w}$ and $S_{xx,r}$, when computed with linear (L) and nonlinear (NL) methods for GLOBEX series B1.

The second alternative method only concerns the linear case. Indeed, contrary to the nonlinear approach, the main wave radiation stress term can also be computed following the commonly used spectral definition for unidirectional waves (e.g., Equation 9 of Buckley et al., 2015):

$$S_{xx,w} = \int_{f_{min}}^{f_{max}} \rho g\, \mathcal{S}(f) \left(2\frac{c_g}{c} - \frac{1}{2} \right) df = \int_{f_{min}}^{f_{max}} \rho g\, \mathcal{S}(f) \left(\frac{1}{2} + \frac{2kh}{\sinh(2kh)} \right) df, \tag{31}$$

where f_{min} and f_{max} define the short-wave frequency band, c_g is the group velocity, and $\mathcal{S}(f)$ is the wave power density spectrum. This spectral computation of (linear) $S_{xx,w}$ is thus also considered in the present section.

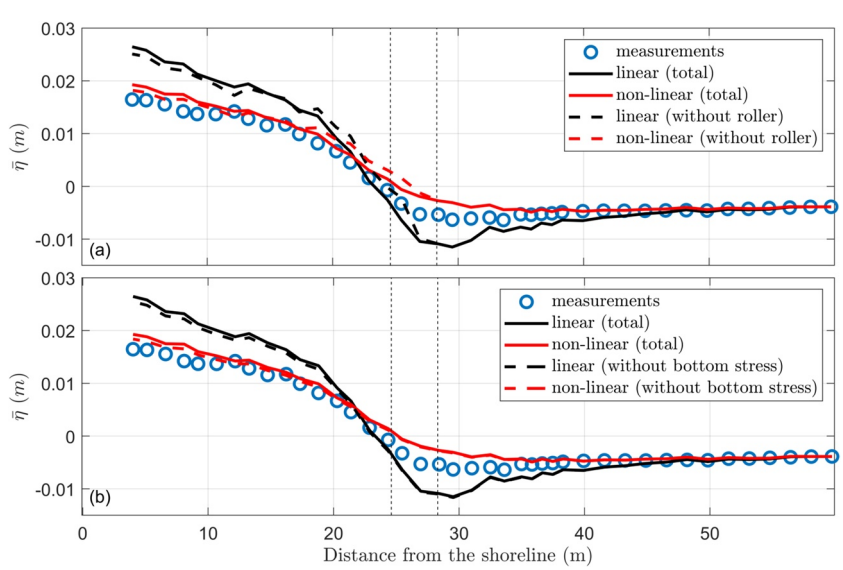

Figure 8. Mean surface elevation modeled: (a) with and without the roller contribution ($S_{xx,r}$), and (b) with and without the bottom stress contribution, for GLOBEX series B1.

Table 5
Contributions of Bottom Stress, Wave Roller, and Main Radiation Stress Term ($S_{xx,w}$) to the Wave Setup Modeled at the Shoreline, for All GLOBEX Test Series

	Bottom stress		Roller		$S_{xx,w}$	
Series	L	NL	L	NL	L	NL
B1	4%	5%	5%	6%	91%	89%
B2	4%	5%	6%	6%	90%	89%
B3	7%	9%	4%	5%	89%	86%
R1	7%	7%	1%	2%	92%	91%
R2	6%	7%	5%	6%	89%	87%
R3	5%	6%	4%	6%	91%	88%

Note. GLOBEX, Gently sLOping Beach EXperiments.

Figure 9 (series B1) and Figure 10 (series R2) show the resulting profiles of wave radiation stress and mean surface elevation obtained using the bulk approach (linear and nonlinear cases) and the spectral approach (linear case). The error statistics (NRMSE) for the mean elevation predicted at the shoreline with these two alternative approaches are given for all test series in Table 6. First, we observe that bulk computations of wave setup are consistent with wave-by-wave computations for both linear and nonlinear methods (compare Table 6 with Table 4), though for random wave conditions the wave-by-wave computations are slightly better than bulk computations in the nonlinear case. Overall, the linear bulk approach still overestimates $\overline{\eta}$ at the shoreline by more than 50% while using the nonlinear bulk approach leads to a decrease in the related NRMSE globally by a factor 2 to 3.

Second, the wave radiation stress profile is significantly reduced when computed following the spectral approach rather than the bulk (or wave-by-wave) approach in the linear case (see Figures 9b and 10b). Associated wave setup predictions are therefore greatly improved, even though they are related to a radiation stress formulation derived from linear theory (i.e., Equation 31). This difference between wave-by-wave and spectral approaches in the linear case is related to the disparity between wave heights obtained from both approaches (see Figures 9a and 10a). Indeed, as short-wave nonlinearity increases (typically around the outer edge of the surf zone), the disparity increases between the H_{rms} obtained from wave-by-wave analysis (Equation 29) and the spectral H_{rms} computed as:

$$H_{rms} = 2\sqrt{2}\sqrt{m_0}, \tag{32}$$

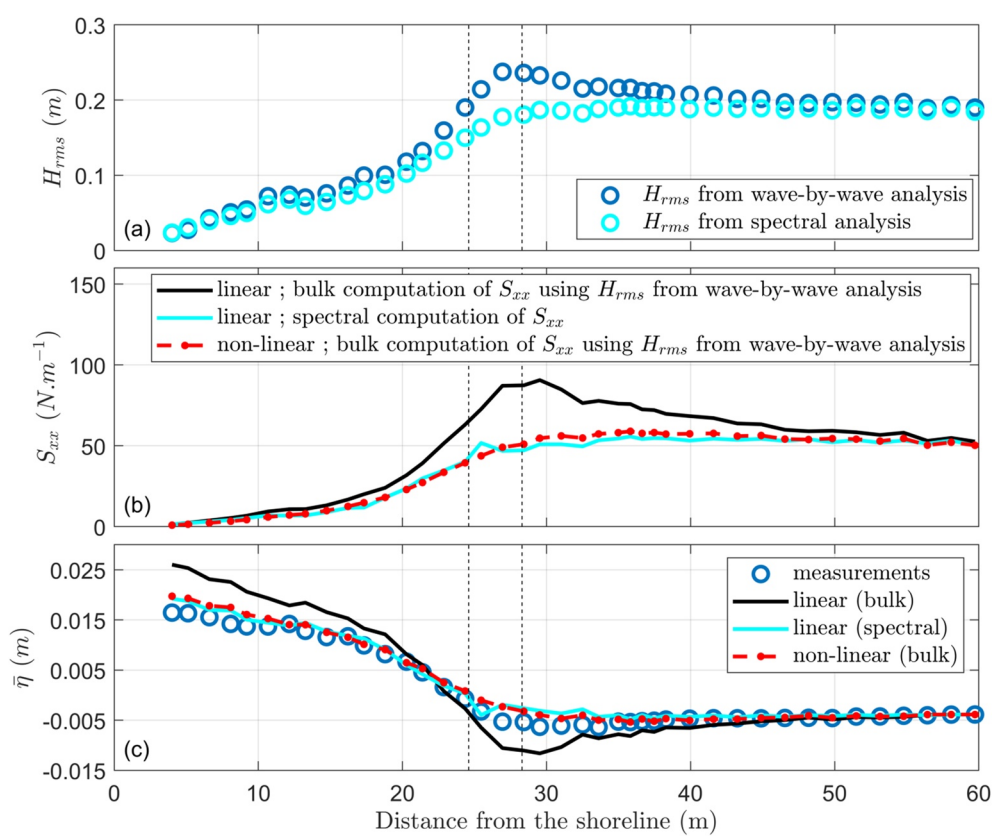

Figure 9. Results for GLOBEX series B1 considering bulk and spectral approaches: (a) root-mean-square wave height (measured), (b) wave radiation stress (modeled), and (c) mean surface elevation (measured and modeled).

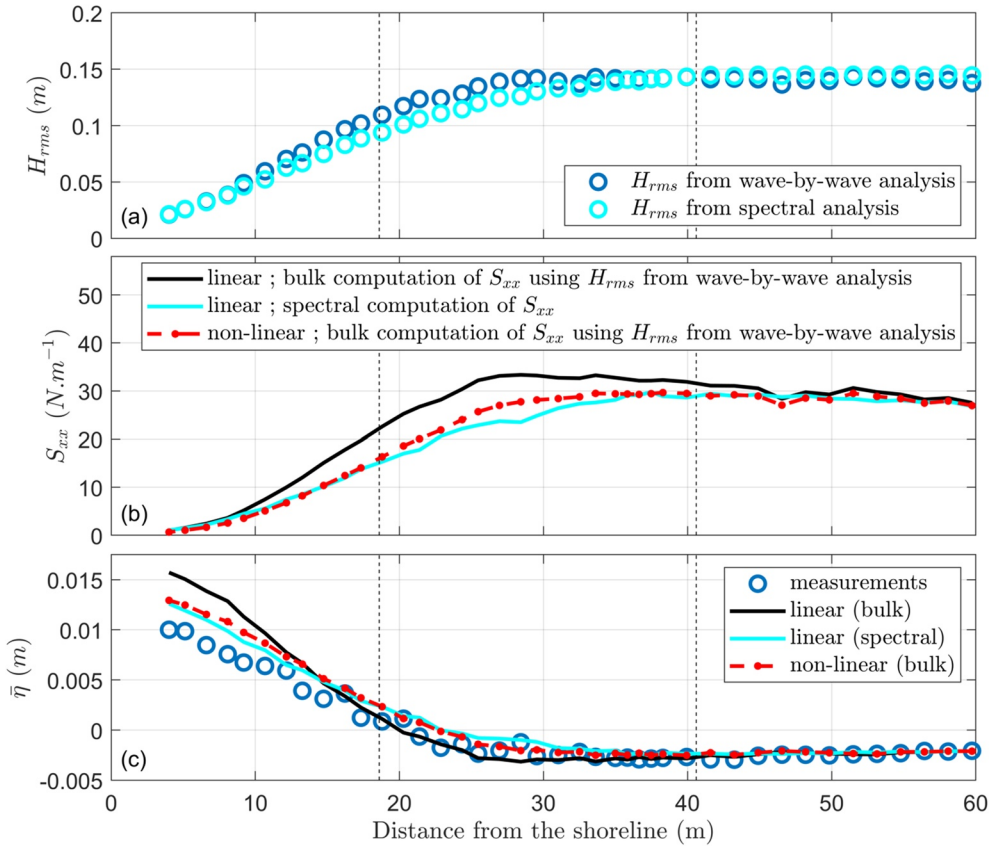

Figure 10. Results for GLOBEX series R2 considering bulk and spectral approaches: (a) root-mean-square wave height (measured), (b) wave radiation stress (modeled), and (c) mean surface elevation (measured and modeled).

with

$$m_0 = \sqrt{\int_{f_{min}}^{f_{max}} \mathcal{S}(f)df}\,. \tag{33}$$

This disparity in wave heights is related to the inherent nature of spectral analysis which decomposes the surface elevation signal into elementary sinusoidal waves, thus becoming more and more inappropriate (regarding the wave height) as short-wave nonlinearity increases. This is clearly explained and illustrated in Section 5.2 of Goda (2010). Michallet et al. (2011) also observed similar differences between significant wave heights obtained from wave-by-wave and spectral analysis (see their Figure 7). While considering the wave-by-wave H_{rms} leads to the correct wave energy in the nonlinear case (hence the consistent and satisfactory results in the nonlinear wave-by-wave and bulk approaches), it leads to overestimating the wave energy in the linear case. In contrast, the fact that spectral analysis gives the correct wave energy greatly improves the prediction of the wave setup in the linear case, despite underestimating the wave height when short-wave nonlinearity is significant.

Table 6
Measured and Predicted Mean Surface Elevation at the Shoreline With Associated NRMSE, for Linear (Bulk and Spectral) and Nonlinear (Bulk) Approaches

Series	$\bar{\eta}_{meas}$ (shoreline)	$\bar{\eta}_{pred}$ and NRMSE (shoreline)		
		L (bulk)	L (spectral)	NL (bulk)
B1	1.65 cm	2.60 cm; +58%	1.92 cm; +16%	1.97 cm; +19%
B2	1.67 cm	2.56 cm; +53%	1.96 cm; +17%	1.97 cm; +18%
B3	1.28 cm	2.10 cm; +64%	1.61 cm; +26%	1.65 cm; +29%
R1	0.38 cm	0.60 cm; +58%	0.47 cm; +24%	0.51 cm; +34%
R2	1.00 cm	1.57 cm; +57%	1.26 cm; +26%	1.29 cm; +29%
R3	0.47 cm	0.76 cm; +62%	0.55 cm; +17%	0.59 cm; +26%

Note. NRMSE, normalized root-mean-square errors.

6. Conclusions

Based on the cross-shore balance equation that links the mean surface elevation with the wave radiation stress (including wave roller) and the bottom stress, a one-dimensional cross-shore model was used in the present work to study the potential effect of accounting for wave nonlinearity

in the prediction of wave setup. Measurements of mean surface elevation from the GLOBEX laboratory data set (Ruessink et al., 2013), involving bichromatic and random wave conditions over a gently sloping beach, were confronted with linear predictions based on the Airy wave theory and with nonlinear predictions based on the stream function theory. A significant improvement was systematically obtained when predicting the wave setup using the nonlinear approach, due to the enhanced representation of instantaneous surface elevation and orbital velocity. In agreement with several previous studies (Garcez Faria et al., 2000; Shabani et al., 2011; Stive & Wind, 1982; Wang et al., 2008) the wave radiation stress appeared higher in the linear case, which led to wave setup overestimations of at least about 50% at the shoreline while this error was reduced globally by a factor 2 to 4 in the nonlinear case.

Contributions of bottom stress, wave roller and main radiation stress term to wave setup predictions were investigated. Overall, the contributions of bottom stress and wave roller appeared secondary compared to the main radiation stress term, since their combined contribution accounts for about 10% of the modeled wave setup at the shoreline for both the linear and nonlinear approaches.

Alternative computational methods were also considered in order to compare with the wave-by-wave approach. For both the linear and nonlinear cases, bulk computations based on the wave-by-wave H_{rms} appeared consistent with the initial wave-by-wave computations. Finally, using a spectral approach in the linear case greatly improved the predictions due to a correct account of the wave energy.

Data Availability Statement

The GLOBEX data used in this work are available through a Zenodo repository (https://doi.org/10.5281/zenodo.4009405).

Acknowledgments
The GLOBEX project was supported by the European Community's Seventh Framework Program through the grant to the budget of the Integrated Infrastructure Initiative Hydralab IV (contract 261520). The authors thank all researchers and Deltares staff members involved in this project. Philippe Bonneton is acknowledged for a brief but enlightening discussion during the preliminary stage of this work. Kévin Martins is warmly acknowledged for sharing his expertize regarding the wave roller. The two anonymous reviewers and the associate editor are sincerely acknowledged for their very valuable feedback. The BW-CGC company is gratefully acknowledged for financially supporting the part-time research work of the first author.

References

Apotsos, A., Raubenheimer, B., Elgar, S., Guza, R., & Smith, J. A. (2007). Effects of wave rollers and bottom stress on wave setup. *Journal of Geophysical Research*, *112*, C02003. https://doi.org/10.1029/2006jc003549

Bertin, X., Fortunato, A. B., & Oliveira, A. (2009). A modeling-based analysis of processes driving wave-dominated inlets. *Continental Shelf Research*, *29*(5–6), 819–834. https://doi.org/10.1016/j.csr.2008.12.019

Bowen, A. J., Inman, D., & Simmons, V. (1968). Wave 'set-down' and set-up. *Journal of Geophysical Research*, *73*(8), 2569–2577. https://doi.org/10.1029/jb073i008p02569

Buckley, M. L., Lowe, R. J., Hansen, J. E., & Van Dongeren, A. R. (2015). Dynamics of wave setup over a steeply sloping fringing reef. *Journal of Physical Oceanography*, *45*(12), 3005–3023. https://doi.org/10.1175/jpo-d-15-0067.1

Chappelear, J. (1961). Direct numerical calculation of wave properties. *Journal of Geophysical Research*, *66*(2), 501–508. https://doi.org/10.1029/jz066i002p00501

Dally, W. R., & Brown, C. A. (1995). A modeling investigation of the breaking wave roller with application to cross-shore currents. *Journal of Geophysical Research*, *100*(C12), 24873–24883. https://doi.org/10.1029/95jc02868

Dally, W. R., & Dean, R. G. (1984). Suspended sediment transport and beach profile evolution. *Journal of Waterway, Port, Coastal, and Ocean Engineering*, *110*(1), 15–33. https://doi.org/10.1061/(asce)0733-950x(1984)110:1(15)

Dean, R. G. (1965). Stream function representation of nonlinear ocean waves. *Journal of Geophysical Research*, *70*(18), 4561–4572. https://doi.org/10.1029/jz070i018p04561

de Bakker, A., Herbers, T., Smit, P., Tissier, M., & Ruessink, B. (2015). Nonlinear infragravity–wave interactions on a gently sloping laboratory beach. *Journal of Physical Oceanography*, *45*(2), 589–605. https://doi.org/10.1175/jpo-d-14-0186.1

Dyhr-Nielsen, M., & Sørensen, T. (1970). Some sand transport phenomena on coasts with bars. *Proceedings of Coastal Engineering*, 855–865. https://doi.org/10.1061/9780872620285.054

Fenton, J. D. (1988). The numerical solution of steady water wave problems. *Computers & Geosciences*, *14*(3), 357–368. https://doi.org/10.1016/0098-3004(88)90066-0

Fenton, J. D. (1999). Numerical methods for nonlinear waves. *Advances in Coastal and Ocean Engineering*, *5*, 241–324. https://doi.org/10.1142/9789812797544_0005

Fortunato, A. B., Freire, P., Bertin, X., Rodrigues, M., Ferreira, J., & Liberato, M. L. (2017). A numerical study of the February 15, 1941 storm in the Tagus estuary. *Continental Shelf Research*, *144*, 50–64. https://doi.org/10.1016/j.csr.2017.06.023

Garcez Faria, A., Thornton, E., Lippmann, T., & Stanton, T. (2000). Undertow over a barred beach. *Journal of Geophysical Research*, *105*(C7), 16999–17010. https://doi.org/10.1029/2000jc900084

Goda, Y. (2010). Reanalysis of regular and random breaking wave statistics. *Coastal Engineering Journal*, *52*(1), 71–106. https://doi.org/10.1142/s0578563410002129

Guérin, T., Bertin, X., Coulombier, T., & de Bakker, A. (2018). Impacts of wave-induced circulation in the surf zone on wave setup. *Ocean Modelling*, *123*, 86–97. https://doi.org/10.1016/j.ocemod.2018.01.006

Guérin, T., de Bakker, A., & Bertin, X. (2019). On the bound wave phase lag. *Fluids*, *4*(3), 152. https://doi.org/10.3390/fluids4030152

Holthuijsen, L. H. (2010). *Waves in oceanic and coastal waters*. Cambridge university press.

James, I. (1974). Non-linear waves in the nearshore region: Shoaling and set-up. *Estuarine and Coastal Marine Science*, *2*(3), 207–234. https://doi.org/10.1016/0302-3524(74)90013-9

Kennedy, A. B., Westerink, J. J., Smith, J. M., Hope, M. E., Hartman, M., Taflanidis, A. A., et al. (2012). Tropical cyclone inundation potential on the Hawaiian Islands of Oahu and Kauai. *Ocean Modelling*, *52*, 54–68. https://doi.org/10.1016/j.ocemod.2012.04.009

Lippmann, T., Brookins, A. S., & Thornton, E. (1996). Wave energy transformation on natural profiles. *Coastal Engineering*, *27*(1–2), 1–20. https://doi.org/10.1007/978-3-642-80292-8_1

Longuet-Higgins, M. S., & Stewart, R. (1964). Radiation stresses in water waves; a physical discussion, with applications. *Deep Sea Research and Oceanographic Abstracts*, *11*(4), 529–562. https://doi.org/10.1016/0011-7471(64)90001-4

Malarkey, J., & Davies, A. (2012). A simple procedure for calculating the mean and maximum bed stress under wave and current conditions for rough turbulent flow based on method. *Computers & Geosciences*, *43*, 101–107. https://doi.org/10.1016/j.cageo.2012.02.020

Martins, K., Blenkinsopp, C., Deigaard, R., & Power, H. E. (2018). Energy dissipation in the inner surf zone: New insights from LiDAR-based roller geometry measurements. *Journal of Geophysical Research: Oceans*, *123*, 3386–3407. https://doi.org/10.1029/2017jc013369

Mastenbroek, C., Burgers, G., & Janssen, P. (1993). The dynamical coupling of a wave model and a storm surge model through the atmospheric boundary layer. *Journal of Physical Oceanography*, *23*(8), 1856–1866. https://doi.org/10.1175/1520-0485(1993)023<1856:TDCOAW>2.0.CO;2

Michallet, H., Cienfuegos, R., Barthélemy, E., & Grasso, F. (2011). Kinematics of waves propagating and breaking on a barred beach. *European Journal of Mechanics-B/Fluids*, *30*(6), 624–634. https://doi.org/10.1016/j.euromechflu.2010.12.004

Nicolae-Lerma, A., Pedreros, R., Robinet, A., & Sénéchal, N. (2017). Simulating wave setup and runup during storm conditions on a complex barred beach. *Coastal Engineering*, *123*, 29–41. https://doi.org/10.1016/j.coastaleng.2017.01.011

Raubenheimer, B., Guza, R., & Elgar, S. (2001). Field observations of wave-driven setdown and setup. *Journal of Geophysical Research*, *106*(C3), 4629–4638. https://doi.org/10.1029/2000jc000572

Rienecker, M., & Fenton, J. (1981). A Fourier approximation method for steady water waves. *Journal of Fluid Mechanics*, *104*, 119–137. https://doi.org/10.1017/s0022112081002851

Rijnsdorp, D. P., Buckley, M. L., da Silva, R. F., Cuttler, M. V., Hansen, J. E., Lowe, R. J., et al. (2021). A numerical study of wave-driven mean flows and setup dynamics at a coral reef-lagoon system. *Journal of Geophysical Research: Oceans*, *126*, e2020JC016811. https://doi.org/10.1029/2020jc016811

Ruessink, B. G., Michallet, H., Bonneton, P., Mouazé, D., Lara, J., Silva, P. A., & Wellens, P. (2013). GLOBEX: Wave dynamics on a gently sloping laboraty beach. *Proceedings of Coastal Dynamics*, 1351–1362.

Savage, R. P. (1957). Model tests for hurricane protection project. In *Bulletin of the Beach Erosion Board, US Army Corps of Engineers*, Washington, DC.

Saville, T. (1961). Experimental determination of wave set-up. In *Proceedings of Second Technology Conference on Hurricanes, US Department of Commerce, National Hurricane Research Project*, 242–252.

Shabani, B., Nielsen, P., & Baldock, T. E. (2011). Wave setup: A non-linear approach. *The Twenty-first International Offshore and Polar Engineering Conference*, *3*, 853–860.

Soulsby, R., & Clarke, S. (2005). *Bed shear-stress under combined waves and currents on smooth and rough beds*. Technical Report 137, HR Wallingford, Wallingford.

Stive, M. J., & Wind, H. (1986). Cross-shore mean flow in the surf zone. *Coastal Engineering*, *10*(4), 325–340. https://doi.org/10.1016/0378-3839(86)90019-0

Stive, M. J., & Wind, H. G. (1982). A study of radiation stress and set-up in the nearshore region. *Coastal Engineering*, *6*(1), 1–25. https://doi.org/10.1016/0378-3839(82)90012-6

Svendsen, I. A. (1984). Wave heights and set-up in a surf zone. *Coastal Engineering*, *8*(4), 303–329. https://doi.org/10.1016/0378-3839(84)90028-0

Wang, B., Chadwick, A. J., & Otta, A. K. (2008). Derivation and application of new equations for radiation stress and volume flux. *Coastal Engineering*, *55*(4), 302–318. https://doi.org/10.1016/j.coastaleng.2007.11.008

Wolf, J. (2009). Coastal flooding: Impacts of coupled wave–surge–tide models. *Natural Hazards*, *49*(2), 241–260. https://doi.org/10.1007/s11069-008-9316-5

Wu, G., Shi, F., Kirby, J. T., Liang, B., & Shi, J. (2018). Modeling wave effects on storm surge and coastal inundation. *Coastal Engineering*, *140*, 371–382. https://doi.org/10.1016/j.coastaleng.2018.08.011

Ye, F., Zhang, Y. J., Yu, H., Sun, W., Moghimi, S., Myers, E., et al. (2020). Simulating storm surge and compound flooding events with a creek-to-ocean model: Importance of baroclinic effects. *Ocean Modelling*, *145*, 101526. https://doi.org/10.1016/j.ocemod.2019.101526